Malassezia responds to environmental pH signals through the conserved Rim/Pal pathway

Kaila M. Pianalto [1,2], Calla L. Telzrow [1,2], Hannah Brown Harding [1,2], Jacob T. Brooks [6], Joshua A. Granek [2,3], Eduardo Gushiken-Ibañez [8,9], Salomé LeibundGut-Landmann [8,9], Joseph Heitman [1,2,4,5], *Giuseppe Ianiri [7], and *J. Andrew Alspaugh [1,2,5]

Departments of Medicine[1], Molecular Genetics and Microbiology[2], Biostatistics and Bioinformatics[3], Pharmacology and Cancer Biology[4], and Cell Biology[5]; Duke University School of Medicine, Durham, NC, USA;
Department of Physics and Astronomy[6], University of North Carolina, Chapel Hill, NC, USA;
Department of Agricultural, Environmental and Food Sciences[7], Università degli Studi del Molise, Italy;
Section of Immunology at Vetsuisse Faculty [8], and Institute of Experimental Immunology[9], University of Zurich, Switzerland

Current affiliations:
Kaila M. Pianalto
KBI Biopharma
Durham, NC, USA

Calla L. Telzrow
PPD, Part of Thermo Fisher Scientific
High Point, NC, USA

Hannah Brown Harding
Department of Medicine
Massachusetts General Hospital, Harvard Medical School,
Cambridge, MA, USA

Jacob T. Brooks
Department of Physics and Astronomy
High Point University, High Point, NC, USA

*Co-corresponding authors:
Giuseppe Ianiri
Via De Sanctis SNC
Department of Agricultural, Environmental and Food Sciences
Università degli Studi del Molise
86100 Campobasso (CB), Italy
giuseppe.ianiri@unimol.it
J. Andrew Alspaugh
303 Sands Research Building
DUMC 102359
Duke University School of Medicine
Durham, NC. USA. 27710
andrew.alspaugh@duke.edu

Abstract

During mammalian colonization and infection, microorganisms must be able to rapidly sense and adapt to changing environmental conditions including alterations in extracellular pH. The fungus-specific Rim/Pal signaling pathway is one process that supports microbial adaptation to alkaline pH. This cascading series of interacting proteins terminates in the proteolytic activation of the highly conserved Rim101/PacC protein, a transcription factor that mediates microbial responses that favor survival in neutral/alkaline pH growth conditions, including many mammalian tissues. We identified the putative Rim pathway proteins Rim101 and Rra1 in the human skin colonizing fungus *Malassezia sympodialis*. Gene deletion by transconjugation and homologous recombination revealed that Rim101 and Rra1 are required for *M. sympodialis* growth at higher pH. Additionally, comparative transcriptional analysis of the mutant strains compared to wild-type suggested mechanisms for fungal adaptation to alkaline conditions. These pH-sensing signaling proteins are required for optimal growth in a murine model of atopic dermatitis, a pathological condition associated with increased skin pH. Together these data elucidate both conserved and phylum-specific features of microbial adaptation to extracellular stresses.

62 **Importance**

63 The ability to adapt to host pH has been previously associated with microbial virulence in several
64 pathogenic fungal species. Here we demonstrate that a fungal-specific alkaline response pathway is
65 conserved in the human skin commensal fungus *Malassezia sympodialis* (*Ms*). This pathway is
66 characterized by the pH-dependent activation of the Rim101/PacC transcription factor that controls cell
67 surface adaptations to changing environmental conditions. By disrupting genes encoding two predicted
68 components of this pathway, we demonstrated that the Rim/Pal pathway is conserved in this fungal
69 species as a facilitator of alkaline pH growth. Moreover, targeted gene mutation and comparative
70 transcriptional analysis supports the role of the *Ms* Rra1 protein as a cell surface pH sensor conserved
71 within the basidiomycete fungi, a group including plant and human pathogens. Using an animal model of
72 atopic dermatitis, we demonstrate the importance of *Ms* Rim/Pal signaling in this common
73 inflammatory condition characterized by increased skin pH.
74

Introduction

Changes in temperature, nutrient availability, or environmental pH create stressful conditions for microorganisms requiring continuous cellular adaptation for survival. In the case of pathogenic organisms, the shift from the ambient environment to the human host results in changes in many of these conditions, in addition to exposure to the host immune system. Similarly, commensal microorganisms must adapt to the unique environmental stresses presented by their specific niches within the host.

Extracellular pH can vary widely as microbes move from the environment to the human host. Even within the human body, pH can vary from the acidic pH of the stomach, to the more neutral pH of blood, to the basic pH of bile. Human skin tends to be more acidic than blood or other body sites, with pH levels that can vary from pH 4 to pH 6 on healthy adult skin [1]. This is an ideal pH for optimal growth of many fungi including *Malassezia sympodialis* (*Ms*) [2], a skin commensal microbe and opportunistic pathogen. However, in inflammatory skin conditions such as atopic dermatitis, the skin pH increases, representing an environmental trigger for this yeast-like species [2]. Additionally, other *Malassezia* species are adapted for colonization of the human gut. Recent reports reported that *Malassezia* can migrate from the more acidic upper gastrointestinal tract to more alkaline micro-niches in the pancreas, demonstrating how certain fungal species can adapt to fluctuations of pH within a mammalian host [3].

The fungus-specific Rim/Pal pathway includes a conserved cascading series of interacting proteins that sense and respond to changes in pH [4-6]. First described in model ascomycete fungi such as *Saccharomyces cerevisiae* and *Aspergillus nidulans*, this signaling pathway initiates a response to pH changes at the cell surface through the Rim21/PalH pH sensor [7-9]. This signal is then propagated through a conserved signaling cascade, with eventual cleavage and activation of the Rim101/PacC zinc-finger transcription factor [10-12]. Once activated, this transcription factor translocates to the nucleus where it regulates the expression of many genes, resulting in an adaptive cellular response to alkaline

pH stress [6, 10, 13, 14]. By convention, this pathway has been referred to as the Pal pathway in filamentous fungi, and as the Rim pathway in fungi that grow predominantly as yeasts, such as *Saccharomyces cerevisiae*, *C. albicans*, and *C. neoformans*. Studies of this pathway in pathogenic fungi have revealed that many virulence factors require Rim/Pal pathway activation in order to be expressed. For example, in *Candida albicans*, the Rim pathway is required for the yeast-hyphal transition that is necessary for tissue invasion [15, 16]. Additionally, in the basidiomycete fungus *Cryptococcus neoformans*, activation of the Rim pathway is required for full expression of many virulence-associated phenotypes, including induction of the polysaccharide capsule and the formation of titan cells [10, 14, 17, 18].

Many Rim/Pal pathway proteins are conserved between the ascomycete fungi and the basidiomycete fungi *Cryptococcus neoformans* and *Ustilago maydis*, such as the components of the proteolysis complex (Rim20/PalA, Rim23/PalC, and the Rim13/PalB protease) and the Rim9/PalI chaperone [18-20]. Homologs of more upstream components comprising the pH-sensing complex, including the Rim21/PalH pH sensor and the Rim8/PalF arrestin, are notably absent in the genomes of basidiomycetes [18, 19]. The *C. neoformans* Rra1 protein was recently identified as a cell surface-associated protein that acts upstream of the Rim proteolysis complex to activate this pathway. While lacking sequence homology with the ascomycete Rim21 protein, *Cn* Rra1 shares functional and structural similarities with this established pH sensor [18] . Importantly, while Rim21 homologs are absent from the genomes of many basidiomycete fungi, Rra1 homologs are readily apparent in sequenced basidiomycete genomes [18]. We also identified a novel Rra1 interactor, Nucleosome Assembly Protein 1 (Nap1), which is required for activation of the Rim pathway in *C. neoformans*. However, Nap1 homologs do not appear to be similarly involved in the Rim pathway of *S. cerevisiae* [21]. We therefore explored the degree of functional conservation of potential Rim pathway proteins in other basidiomycetes, such as *M. sympodialis*.

In this study, we established that the *M. sympodialis* Rim101 transcription factor and the putative Rra1 pH sensor are each required for survival at alkaline pH. In this way, we demonstrated that Rra1 is likely a conserved, basidiomycete-specific Rim pathway component. We also examined the transcriptional output of the *M. sympodialis* Rim pathway at alkaline pH, giving insight into the cellular processes involved in *M. sympodialis* survival in this stressful condition. Finally, we validated the relevance of the *Ms* Rim pathway in the interaction of this commensal fungus with the host by examining the innate immune response to fungal challenge *in vitro* and by evaluating the fitness of the fungus in the atopic skin environment *in vivo*.

Materials and Methods

Strains, media, and growth conditions. Strains used in this study are listed in **Supplemental Table S1**. Strains were routinely grown on modified Dixon's (mDixon) medium (3.6% malt extract (Bacto), 1% mycological peptone (Oxoid), 1% ox bile (HiMedia), 1% v/v Tween 60 (Sigma), 0.4% glycerol; 2% Bacto agar added for plates) [22, 23]. For mDixon medium that was adjusted to specific pH, 150 mM HEPES was added to the medium as a buffering agent, and the pH was adjusted by addition of either concentrated HCl or NaOH. For *in vivo* experiments, strains were grown in a differently modified Dixon medium containing 3.6% malt extract (Sigma), 2% ox bile (Sigma), 0.6% bacterial peptone (Oxoid), 1% Tween 40 (Sigma), 0.2% glycoreol (Sigma) and 0.2% oleic acid (Sigma) [24]. Strains were cultured at 30˚C unless otherwise indicated. *Agrobacterium tumefaciens* cultures were maintained on YT agar or FB broth (YT agar: 0.8% Bacto tryptone, 0.5% Yeast Extract, 0.5% NaCl, 1.5% glucose; FB broth: 2.5% Bacto tryptone, 0.75% yeast extract, 0.1% glucose, 0.6% NaCl, 50 mM Tris-HCl pH 7.6) at 30˚C.

Agrobacterium tumefaciens-mediated transformation. The *M. sympodialis RIM101* and *RRA1* genes were identified in the *M. sympodialis* genome assembly via BLASTp analysis [25]. To generate *M. sympodialis mutants*, targeted deletion constructs consisting of 1.5 kb of genomic sequence upstream and downstream the target genes and the *NAT* resistance marker were cloned into the T-DNA regions of plasmid pGI3 [26] using in vivo recombination in *Saccharomyces cerevisiae* as previously described [23]. Primers used to create the deletion constructs can be found in **Supplemental Table S2**. The resulting plasmid was transformed into *A. tumefaciens* EHA105 via electroporation and subsequent selection on YT agar supplemented with 50 µg/mL kanamycin.

Agrobacterium-mediated transformation was performed as described previously with some modifications [23, 27]. Briefly, *M. sympodialis* ATCC 42132 was incubated for 2 days at 30˚C in mDixon liquid medium, and *A. tumefaciens* strains containing pKP38 (*RIM101* deletion) or pKP39 (*RRA1* deletion)

were incubated overnight in FB + kanamycin at 30˚C. *A. tumefaciens* cultures were diluted to an OD_{600} of 1 in Induction Medium (IM) (335) and incubated a further 4 hours at 30˚C. *M. sympodialis* cells and induced *A. tumefaciens* cells were mixed at a 5:1 *Malassezia* : *Agrobacterium* ratio and pelleted at 5000 rpm, 10 min. The resulting cell pellet was spotted onto nylon membranes on modified IM (mIM) plates (IM medium supplemented with 0.4% ox bile, 0.4% v/v Tween 60 (Sigma), 0.1% v/v Tween 20) and incubated at RT for 7 days. After 7 days, cells were scraped from the membranes into sterile H_2O and pelleted at 3000 rpm for 5 minutes (to preferentially pellet the *Malassezia* cells over the *Agrobacterium* cells). The resulting pellets were resuspended in sterile H_2O and spread onto mDixon medium with cefotaxime + either nourseothricin or neomycin (300 µg/mL cefotaxime; 100 µg/mL nourseothricin; 200 µg/mL neomycin G418).

Resulting colonies were screened by PCR to confirm homologous recombination of the gene deletion constructs into the endogenous locus using primers listed in **Supplemental Table S3** [21]. Independent mutant strains for each gene were made by separate, completely independent transformations. All tested phenotypes were concordant between independent mutant strains; therefore, results from single or both mutants for each gene are demonstrated in the Results.

Quantitative reverse-transcriptase PCR. As a pilot experiment prior to RNA sequencing, *M. sympodialis RIM101* expression was measured via RT-qPCR, per previous methods [21]. *M. sympodialis* was incubated overnight in mDixon at pH 4. Cells were pelleted by centrifugation and washed twice in sterile H_2O, then resuspended in mDixon medium, mDixon buffered to described pH levels, RPMI + 10% FBS, or DMEM + 10% FBS. *M. sympodialis* was incubated in these media at 30˚C for 90 minutes. At this time, *M. sympodialis* samples were pelleted by centrifugation for 5 minutes at 4000 rpm, 4˚C. Cells were washed 2X with cold sterile H_2O, then flash frozen on dry ice. RNA was purified using Trizol phenol-chloroform extraction (Invitrogen). cDNA was prepared using the AffinityScript cDNA synthesis kit (Agilent). qRT-PCR

was performed using PowerUp SYBR Green (ThermoFisher). Relative *MsRIM101* gene expression levels compared to pH 4 conditions were calculated using the $\Delta\Delta C_T$ method with the *MsTUB1* tubulin gene as control [21]**.** RT-PCR primers for the *MsRIM101* and *MsTUB1* genes can be found in **Supplemental Table S4**.

RNA Sequencing. To prepare samples for RNA sequencing, *M. sympodialis* WT, *rim101*Δ, and *rra1*Δ strains were grown in biological triplicate for 18 h in mDixon liquid medium at 30˚C. Cultures were pelleted at 4000 rpm for 10 min, washed 1X with sterile H_2O, and resuspended at an OD_{600} of 2.5 in 20 mL of mDixon pH 4 (Rim pathway-inactivating condition), mDixon pH 7.5 (Rim pathway-activating condition), or DMEM supplemented with 10% FBS ("host-like" condition). Cultures were incubated at 30˚C for 90 minutes with shaking. Cultures were harvested by centrifugation at 4000 rpm for 10 min at 4˚C, then washed once with cold sterile H_2O. Cell pellets were flash frozen in a dry ice-ethanol bath and lyophilized overnight. RNA was extracted from the lyophilized pellets via a Trizol-chloroform extraction (Invitrogen). The resulting RNA was treated with DNase I (New England Biolabs) for 30 min at 37˚C as described, then re-purified using Trizol and chloroform.

RNA Sequencing was performed in collaboration with the Duke University Center for Genomic and Computational Biology Sequencing and Genomic Technology Shared Resource. An mRNA library was prepared using a Kapa Stranded mRNA-Seq library prep kit. Stranded mRNA-Seq was performed on an Illumina HiSeq 4000 with 50-bp single-end reads. Reads were mapped to the *M. sympodialis* ATCC 42132 reference genome (obtained from Ensembl, accessed March 2021) using STAR alignment software [28]. Differential expression analyses were performed in R using a RNA-Seq Bioconductor workflow [29], followed by the DESeq2 package [30]. Genes were considered statistically differentially expressed if they had an adjusted P value [false-discovery rate (FDR)] of <0.05. Functional prediction for differentially

regulated genes (+/- 1 log2 fold change) was performed using Fungi DB (www.fungidb.org [Release 63]) [31] entering the MSYG gene identifier for each transcript of interest.

The test of correlation between fold change values for *rra1*Δ and *rim101*Δ mutants was calculated using Kendall's τ test, with the alternative hypothesis that fold change values were positively correlated. We initially only considered genes with significantly differential expression (adjusted p-value <= 0.05) in both mutants relative to WT. Results for among genes with significant differences in expression, using Kendall's τ, of gene expression in between the growth at pH 7.5, in DMEM, and at pH 4 were, respectively, τ= 0.8206107, p-value < 2.2x10-16; τ= 0.71747, p-value < 2.2x10-16; τ= 1, p-value = 0.1666667). Because there are only 3 genes that have significantly different expression in at pH 4 (in both *rra1*Δ and *rim101*Δ mutants compared to WT), we repeated this calculation for all genes and again found significant results (with less dramatic τ values) for growth at pH 7.5 and in DMEM, but, again, not at pH 4 ((respectively τ= 0.6022764, p-value < 2.2x10-16; τ= 0.5515425, p-value < 2.2x10-16; τ= -0.0465178, p-value = 0.999999). This analysis used the R packages: readxl, dplyr, ggplot2, and patchwork.

Fungal survival in macrophages. The ability of the fungal strains to survive in the presence of macrophages was assessed by co-culture as previously described, with some alterations to accommodate *M. sympodialis* growth requirements [32] [33]. Approximately 10^5 J774A.1 murine macrophages suspended in DMEM (Thermo Fisher Scientific) were added to individual wells of a 96-well plate and incubated overnight at 37°C with 5% CO_2. Following adherence to the 96-well plate, J774A.1 murine macrophages were activated with 10 nM phorbol myristate acetate (PMA) in RPMI 1640 medium (Corning) supplemented with 20% FBS for 1 hour at 37°C with 5% CO_2. Following macrophage activation, *M. sympodialis* strains (WT, *rim101*Δ mutant strains [KPY34 and KPY36], and *rra1*Δ mutant strains [KPY38 and KPY39]), which had been incubated for 48 hours in mDixon medium, were washed

three times in sterile water, normalized to an OD of 0.3 in RPMI 1640 medium supplemented with 20% FBS, and added to the activated J774A.1 murine macrophages (5 x 10^6 fungal cells per well (10:1 fungal cells:macrophages)). Co-cultures of J774A.1 murine macrophages and fungal cells were incubated for 4 hours at 37°C with 5% CO_2. Phagocytosed fungal cells were collected by washing individual wells of the 96-well plate vigorously with sterile water. Collected fungal cells were plated onto mDixon agar to assess the number of viable *M. sympodialis* cells by quantitative culture. The results are reported as the average percentage (± SEM) of recovered CFU, normalized to the WT strain, generated from at least 3 biological replicates. Statistical significance was determined using one-way analysis of variance (ANOVA) and the Tukey-Kramer test (GraphPad Software, San Diego, CA).

Supplementation with 20% FBS provided exogenous lipids to support *M. sympodialis* lipid auxotrophy in this assay. RPMI 1640 medium was utilized specifically in this experiment to limit the impact of alkaline pH on the survivability of the *rim101*Δ and *rra1*Δ mutant strains. We found that a 4-hour incubation in RPMI 1640 medium supplemented with 20% FBS without J774A.1 murine macrophages did not impact the survivability of the *rim101*Δ and the *rra1*Δ mutant strains compared to the WT strain. Attempts at longer incubations, such as 24 hours, failed to recover viable fungi from co-culture. As a result, we used 4-hour co-cultures to directly assess the ability of the tested fungal strains to interact with and survive in the presence of macrophages.

Macrophage activation assays. Bone marrow cells were isolated from C57BL/6 mice (Jackson Laboratories) as previously described [34, 35]. Briefly, femurs were isolated from CO_2-euthanized mice, and each bone marrow space was flushed with cold PBS. Red blood cells were lysed in 1x RBC lysis buffer, and the remaining bone marrow cells were resuspended in 1x Dulbecco's modified Eagle's medium (DMEM) with 1 U/ml penicillin/streptomycin (PenStrep). Adherent cells were differentiated in BMM medium (1x DMEM, 10% fetal bovine serum [FBS; non-heat inactivated], 1 U/ml

penicillin/streptomycin) with 3 ng/ml recombinant mouse GM-CSF (rGM-CSF; R&D Systems or BioLegend) at a concentration of 2.5 x 10^5 cells/ml in 150 x 15 mm petri plates at 37°C with 5% CO_2. The media was refreshed after 3 days and the cells were harvested on day 7 as previously described, likely resulting in a mixture of bone-marrow-derived macrophages (BMMs) and dendritic cells (DCs) [35]. These cells were counted (by hemocytometer, with Trypan blue to differentiate between live and dead cells), plated in BMM medium in 96-well plates at a concentration of 5 x 10^4 cells per well, and incubated at 37°C with 5% CO_2 overnight prior to fungal co-culture experiments.

BMM co-cultures with wildtype *M. sympodialis*, *C. neoformans,* and *C. albicans* as well as *M. sympodialis rim101*Δ and *rra1*Δ mutant strains were performed as described previously [34, 35]. *M. sympodialis* strains (WT (ATCC 42132), *rim101*Δ (KPY34), and *rra1*Δ (KPY36)) were incubated for 3 days in DMEM media supplemented with 10% fetal bovine serum [FBS; non-heat inactivated] and 1 U/ml penicillin/streptomycin) at 30°C. The *C. neoformans* H99 strain was incubated for 2 days in DMEM media supplemented with 10% fetal bovine serum [FBS; non-heat inactivated] and 1 U/ml penicillin/streptomycin) at 30°C. Prior to co-culturing with BMMs, these cultures were transferred to 37°C for 16 hours. WT *C. albicans* (SC5314) cells were incubated for 1 day in DMEM without serum at 30°C prior to co-culture to avoid premature filamentation. Following these incubations, fungal cells were washed twice with PBS, counted, and added to wells of a 96-well plate containing BMM (5 x10^5 BMM/well) at a concentration of 5 x 10^6 fungal cells per well (10:1 fungal cells:BMMs). Co-cultures were incubated for the indicated amount of time (either 3 or 6 hours) at 37°C with 5% CO_2. Supernatants were collected and stored at -80°C overnight. Secreted cytokines (TNF) were quantified in supernatants by enzyme-linked immunosorbent assay (ELISA MAX:Deluxe Set Mouse TNF); BioLegend). Data are represented as the average TNF levels (pg/ml) for 4-5 biological replicates per group [34, 35].

Scanning electron microscopy (SEM). SEM was used to visualize the interactions between *M. sympodialis* strains and J774A.1 murine macrophages. Co-cultures were performed as described above, with some alterations. Individual ethanol-sterilized polydopamine coated coverslips (18 mm diameter) were placed into the wells of a 12-well plate. Approximately 5 x 10^6 J774A.1 murine macrophages suspended in RPMI 1640 medium supplemented with 20% FBS and 10 nM PMA were added to each well and incubated for 1 hour at 37°C with 5% CO_2. Following adherence and activation, 48-hour incubated *M. sympodialis* cultures (WT, *rim101*Δ mutant [KPY34], and *rra1*Δ mutant [KPY38]) were washed three times in sterile water, normalized to an OD of 0.3 in RPMI 1640 medium supplemented with 20% FBS, and added to wells (5 x 10^6 fungal cells per well (1:1 fungal cells:macrophages). Co-cultures of J774A.1 murine macrophages and fungal cells were incubated for 1 hour at 37°C with 5% CO_2 to capture potential interactions (such as phagocytosis) between macrophages and fungal cells.

Co-cultures were fixed with 2.5% glutaraldehyde for 1 hour at room temperature and were subsequently washed 3 times with 1X PBS. Samples were dehydrated by immersing the coverslips in ethanol (30% for 5 minutes, 50% for 5 minutes, 70% for 5 minutes, 95% for 10 minutes, and 100% for 10 minutes performed twice). Samples were then critical point dried with a Tousimis 931 critical point dryer (Rockville, Maryland) and coated with gold-palladium using a Cressington 108 sputter-coater (Watford, United Kingdom). Coverslips containing the prepared samples were mounted and imaged on a Hitachi S-4700 scanning electron microscope (Tokyo, Japan).

Murine skin colonization assay: Mouse experiments in this study were performed in strict accordance with the guidelines of the Swiss Animals Protection Law and under protocols approved by the Veterinary office of the Canton Zurich, Switzerland (license number 142/2021). All efforts were made to minimize suffering and ensure the highest ethical and humane standards according to the 3R principles [36]. WT C57Bl/6JRj mice were purchased from Janvier Elevage (France). All experiments were conducted at the

297 Laboratory Animal Science Center of the University of Zurich under specific pathogen-free conditions.
298 AD-like conditions were induced in the murine ear skin according to Moosbrugger-Martiz et al. [37] and
299 Ruchti et al. [38]. Briefly, 1.125 nm of MC903 (calcipotriol hydrate, Sigma) diluted in pure ethanol was
300 applied on the dorsal and ventral side of both ears for 5 consecutive days and again for 4 days after a
301 resting period of 2 days. The pH in MC903-treated mouse skin is higher (pH 7-7.5) compared to that of
302 control skin (pH 5.5) [39]. *M. sympodialis* strains (WT, *rim101*Δ, and *rra1*Δ) were grown in mDixon for 2
303 days, washed twice in PBS and resuspended in native olive oil. A suspension of 100 µl containing $1x10^7$
304 yeast cells was applied topically onto the dorsal side of both ears while mice were anaesthetized [40].
305 After infection, MC903 treatment was continued on day 2 p.i. (for the 4 days infection experiment) or
306 daily from day 2 to 5 (for the 7 days infection experiment) on the ventral side of the ear only to avoid
307 interference of the EtOH solvent with fungal viability [38]. Ear thickness was continuously monitored
308 using the Oditest S0247 0-5 mm measurement device (Kroeplin). For determining the fungal loads in the
309 skin, the ear tissue was transferred in water supplemented with 0.05% Nonidet P40 (AxonLab),
310 homogenized with a TissueLyzer (Qiagen) for 6 minutes at 25 Hz, plated on mDixon agar, and incubated
311 at 30°C for 3 to 4 days for colony counting.
312
313 Data Accessibility: Processed RNA-seq seq data are available in the supplemental Tables; raw and
314 processed data are available through NCBI Gene Expression Omnibus (GEO) accession number
315 GSE254653 (https://www.ncbi.nlm.nih.gov/geo/query/acc.cgi?acc=GSE254653).
316

Results

Mutants in *M. sympodialis* Rim pathway signaling are hypersensitive to elevated pH and salt concentrations.

In other fungal species, the Rim/Pal pathway is involved in sensing and responding to increases in extracellular pH [4, 5, 14, 18]. Accordingly, Rim pathway genes are required for survival at elevated pH as well as at elevated salt concentrations [15, 17, 41-43]. To determine whether the *M. sympodialis* (*Ms*) Rim pathway is involved in similar cellular responses, two putative Rim pathway genes in the recently annotated *Ms* genome were identified based on sequence homology; MSYG_3336 encodes the closest homolog of the Rim101 transcription factor, and MSYG_4280 encodes the closest homolog of the Rra1 putative pH sensor. To explore their roles in the fungal response to extracellular stresses, two independent loss-of-function mutant strains were generated for each corresponding gene (**Supplemental Table S1**). All tested phenotypes were concordant between the independent *Ms rra1*Δ mutants as well as between the independent *Ms rim101*Δ mutants. On media containing exogenous lipids, the wild-type *Ms* strain was able to grow well from a pH of 5 to a pH of 7.5; the *Ms rim101*Δ and *rra1*Δ mutant strains grew at rates similar to the WT at mildly acidic pH (pH 6) (**Figure 1A**). However, they began to display growth defects at neutral pH 7, and growth was completely inhibited at pH 7.5 (**Figure 1A**). Similar to Rim/Pal pathway mutants in other fungi, these *Ms* mutant strains displayed a growth impairment at high concentrations of NaCl (**Figure 1A**). These results suggest that, as observed in other fungal genera, the *Ms* Rim101 transcription factor is involved in sensing and responding to alkaline pH and high salt conditions. Moreover, these data also suggest that Rra1 homologs play a conserved role in basidiomycete Rim/Pal pathways to sense and respond to alkaline pH signals.

Comparative transcriptional analysis defines Rim pathway-regulated genes in *M. sympodialis*.

Activation of the conserved and fungal-specific Rim signaling pathway results in the proteolytic cleavage of the Rim101 transcription factor, which then translocates to the nucleus to regulate transcriptional responses to alkaline pH, including induction of the expression of *RIM101* itself [14]. To first determine pathway activating signals, we performed quantitative real-time PCR to assess conditions associated with transcriptional activation of the *RIM101* gene. We performed this transcriptional analysis across a gradient of pH values in mDixon medium, while also assessing *RIM101* transcript levels in tissue culture medium. *Ms RIM101* transcript levels increased in response to a more alkaline pH in a dose-dependent manner (**Figure 1B**), similar to *RIM101/PacC* transcriptional induction observed in other fungal species [44, 45]. Additionally, *RIM101* is even more strongly transcriptionally induced in tissue culture media (DMEM and RPMI media, pH 7.4) than mDixon medium pH 7.5, indicating that signals in tissue culture media in addition to pH are involved in activating the Rim pathway in this organism (**Figure 1B**).

We performed deep RNA sequencing comparing the transcriptomes of the *Ms* WT, *rim101*Δ, and *rra1*Δ strains incubated for 90 minutes in mDixon pH 4, mDixon pH 7.5, and DMEM tissue culture medium (pH 7.4). Gene expression is highly correlated between *rra1*Δ and *rim101*Δ mutants, compared to WT, when grown at pH 7.5 or in DMEM, but there is little correlation between *rra1*Δ and *rim101*Δ mutants when they are grown at pH 4 (Figure S1). This correlation is highly statistically significant at pH 7.5 or in DMEM (p-value < 2.2x10-16 for both), but there is no significant correlation for growth at pH 4 (p-value = 0.1666667).

Because there are only three genes that have significantly different expression at pH 4 in both *rra1*Δ and *rim101*Δ mutants compared to WT, we also calculated Kendall's τ for all genes and again found significant results (also less dramatic) for growth at pH 7.5 and in DMEM, but not at pH 4 (respectively τ= 0.6022764, p-value < 2.2x10-16; τ= 0.5515425, p-value < 2.2x10-16; τ= -0.0465178, p-value = 0.999999)

We also analyzed the combined transcriptional data from each experimental sample using multidimensional scaling (MDS) analysis to visually compare variations in the transcriptomes of each dataset. As expected, biological replicates of the same strain incubated at the same conditions tended to cluster more closely to each other than to other samples (**Figure 2A**). This analysis indicates that overall patterns of transcriptional activity are very similar in mDixon medium at pH 4 among the WT, *rim101*Δ, and *rra1*Δ strains (**Figure 2A**), consistent with work in other fungal species demonstrating specific activation of the Rim/Pal pathway in response to alkaline pH and other cell stress signals [4]. In contrast, when these strains were incubated at elevated pH in mDixon medium buffered to pH 7.5 for 90 minutes, there are distinct patterns of transcriptional activity that distinguish the WT strain from the two mutant strains, which clustered together and clearly distinctly from the WT strain (**Figure 2A**). A similar observation was made for samples obtained after growth in DMEM, although there was a higher variation among the *rim101*Δ and *rra1*Δ mutants. The relative transcriptional variation of individual genes between the WT and the *rim101*Δ / *rra1*Δ strains at each pH is demonstrated by Volcano plots (**Figure 2B**).

At pH 4, there are very few genes differentially regulated between the WT and *rim101*Δ or *rra1*Δ mutant strains (**Figure 2B; Tables S5, S6**). However, at pH 7.5, 84 *Ms* genes displayed statistically significant decreased transcript abundance in the *rim101*Δ mutant strain compared to WT (< -1 $\log_2$ fold change), suggesting their transcriptional dependence on the putative Rim101 transcription factor (**Figures 2B, 2C; Tables S7, S8**). Of these genes, 26 (31%) demonstrated similar decreases in transcript abundance in the *rra1*Δ mutant (**Figure 2C; Tables S7, S9, S8, S10, S11**). Additionally, 46 genes displayed increased transcript abundance (> +1 $\log_2$ fold change) in the *rim101*Δ strain compared to WT, and 35 (76%) of these also had increased transcript abundance in the *rra1*Δ strain (**Figures 2B, 2C; Tables S7, S12, S13, S11**).

Similar overlapping transcriptional patterns of the *Ms rim101*Δ and *rra1*Δ mutant strains are observed in DMEM tissue culture medium (pH 7.4): 126 *Ms* genes display decreased transcript abundance in the *rim101*Δ mutant strain compared to WT, and 102 (81%) of these genes also demonstrate decreased transcript abundance in the *rra1*Δ mutant; 63 genes have increased transcript abundance in the *rim101*Δ strain compared to WT, and 54 (86%) have similarly increased transcript abundance in the *rra1*Δ strain (**Figure 2D; Tables S14, S15, S16, S17, S18, S19, S20**).

Assigning likely function to specific genes in these datasets is limited by the incomplete annotation of the *M. sympodialis* genome (>20% of genes listed as encoding an "unspecified product"). However, we used FungiDB [31] to assist in assigning predicted function for the proteins encoded by genes with altered transcription in either the *rim101*Δ or *rra1*Δ mutant strains at pH 7.5 and in DMEM (**Tables S12, S10, S16, S17, S13, S10, S18, S19**). We also manually defined functional categories of predicted function for genes with similar patterns of altered transcription in both the *rim101*Δ and *rra1*Δ strains in these two incubation conditions. A subset of these genes is listed in **Tables 1 and 2**. This analysis suggested potential *Ms* Rim pathway regulation at alkaline pH for multiple genes encoding proteins involved in membrane transport (MFS proteins; transporters of ammonium, amino acids, nucleosides, and ions) and intracellular trafficking (including the ESCRT II protein Vps25). A larger gene set displayed altered transcript abundance in DMEM between the *rim101*Δ / *rra1*Δ strains and WT. These genes similarly included those predicted to encode proteins involved in membrane transport and intracellular trafficking. Additional functional categories for genes with differential transcript abundance in DMEM in these Rim pathway mutants included cell cycle regulation, lipid metabolism, and cell surface modification. These categories are similar to those for Rim pathway-regulated genes in related basidiomycetes in which cell surface (cell wall and membrane) and cell cycle modifications are important components of the adaptive cellular response to environments with elevated pH [45].

The *Ms RRA1* gene displayed transcriptional dependence on the Rim101 transcription factor in DMEM (-0.95 $\log_2$ fold change). This suggests that potentially biologically relevant changes in the transcript abundance of Rim101-regulated genes might be missed by arbitrary fold-change cut-offs and subsequent dataset limitations.

M. sympodialis interacts with macrophages *in vitro* in a Rim pathway-independent manner.

Due to its prevalence on the skin, *Malassezia* species have been studied for interactions with epidermis-resident keratinocytes, dendritic cells, and macrophages [24] as well as with the murine macrophage-like cell line J774A.1 *in vitro* [33]. To assess the role of *M. sympodialis* Rim signaling in the interaction of fungal and innate immune cells, we performed a similar *in vitro* co-culture of the WT and Rim pathway mutants with J774A.1 cells. As early as one hour after co-culture, we observed macrophages clustering with fungal cells (**Figure 3A**). We used scanning electron microscopy (SEM) to further visualize the details of these physical interactions. We found that all tested strains (WT, *rim101*Δ [KPY34], and *rra1*Δ [KPY38]) were actively phagocytosed within one hour of co-culture (**Figure 3B**). Typically, we observed groups of ~2-3 macrophages assembling to engulf clumps of fungal cells. In some cases, the macrophage/fungal cell association contained extracellular material, possibly consistent with macrophage extracellular traps (METs) [46] (**Figure 3B**, yellow arrow heads).

To assess the ability of this macrophage-like cell line to rapidly kill the fungal cells, we also tested for survival differences among the three *M. sympodialis* strains in this co-culture system [33]. We chose a short co-incubation period to address pH-related growth effects in the *rim101*Δ and *rra1*Δ strains. After four hours of co-culture with J774A.1 cells**,** we observed no significant survival differences between the WT, *rim101*Δ, and *rra1*Δ mutants (**Figure 3C, left**). Despite the alkaline pH growth defect of the two mutants, there was no loss of viability of either mutant strain when incubated in tissue culture medium without macrophages during this short period of incubation (**Figure 3C, right**). Collectively,

these observations indicate that macrophages recognize and actively phagocytose *Ms.* However, this association does not result in rapid fungal cell killing.

M. sympodialis elicits a robust TNF response when co-cultured with macrophages independent of Rim pathway signaling**.**

Prior investigations into the ability of *Malassezia* to activate macrophages have yielded conflicting results, with individual studies suggesting that *Malassezia* species may either trigger or inhibit macrophage activation. These discrepancies have been attributed to differences in the growth phase of the cells, the fungal species assayed, and the nature of the protective lipid layer surrounding *Malassezia* cells [47-49]. We quantified the production of tumor necrosis factor (TNF) following co-incubation of primary bone marrow-derived macrophages (BMMs) with the *M. sympodialis* wildtype, *rim101*Δ mutant, and *rra1*Δ mutant strains. We also measured TNF production in response to co-culture with wild-type *Candida albicans* and *Cryptococcus neoformans* strains, to serve as positive and negative controls, respectively. Following both a 3-hour and 6-hour co-culture (**Figure 4A, B**), we observed an expected profound induction of TNF by the macrophages co-cultured with *C. albicans* cells [50]. We also noted undetectable levels of TNF after co-culture with wildtype *C. neoformans* cells, consistent with prior studies documenting an effective immune evasion phenotype by wild-type *C. neoformans* cells [17]. Similar to the case with *C. albicans*, BMMs exposed to all three *M. sympodialis* strains produced high levels of TNF (**Figure 4A, B**). To determine whether this level of TNF by BMMs required viable *M. sympodialis* cells, we repeated the assay with heat-killed fungal cells. We observed similar levels of TNF production as with live cells in all strains tested (**Figure S2**), suggesting that the TNF production is most likely primarily due to a physical interaction between the macrophage and structural features of the fungal cell, as observed in other fungal species [34]. Exposure of the BMMs to the *Ms rra1*Δ mutant strain resulted in variably lower levels of TNF- stimulation compared to the WT and *rim101*Δ mutant,

458 though not resulting in the complete suppression of macrophage activation as observed with the *C.*
459 *neoformans* control (**Figure S2**) [17]. Together these data suggest that the cell changes associated with
460 mutation of the *M. sympodialis RIM101* gene do not affect TNF production by co-cultured macrophages,
461 and a *Ms rra1*Δ mutation has only a partial effect. Moreover, the degree of macrophage TNF production
462 in response to *Ms* is similar to that observed in co-cultures with *C. albicans*. In contrast, *M. sympodialis*
463 does not share the immune avoidance phenotype of *C. neoformans* in this assay.
464
465 The Rim/Pal pathway impacts *M. sympodialis* fitness in a murine model of atopic dermatitis.
466 Finally, we assessed the impact of the Rim/Pal pathway on the interaction of *M. sympodialis* with the
467 host skin *in vivo* under high pH conditions reminiscent of those in the skin of atopic dermatitis patients
468 [39]. Atopy-like conditions were induced by repeated administration of the vitamin D analogue MC903
469 to the murine skin prior to fungal association [39]. WT *M. sympodialis* robustly colonized the murine skin
470 by day 4 post-infection, with higher loads in the atopic dermatitis-like skin than in control skin, as
471 previously shown [38] (**Figure 5A**). Importantly, under high pH, but not low pH conditions, colonization
472 levels of both, the *rim101*Δ [KPY34] and *rra1*Δ [KPY36] mutants were reduced compared to those of the
473 WT control strain, although differences did not reach statistical significance (**Figure 5A**). The effect was
474 more pronounced at day 7, when the lack of *RIM101* and *RRA1* clearly impaired fitness and resistance to
475 clearance of *M. sympodialis* in skin with elevated pH (**Figure 5B**). Overall reduced fungal burden on day 7
476 vs. day 4 is consistent with previous observation that *Malassezia* skin colonization is transient in
477 experimental mice [24, 38]. The diminished capacity of the *rim101*Δ and *rra1*Δ mutants to colonize the
478 atopic dermatitis-like murine skin was not due to an intrinsic growth defect of these strains or a defect
479 to initially establish cutaneous colonization, as they colonized the skin equally well at low pH (**Figure**
480 **5A**). The difference in skin colonization levels between WT, *rim101* and *rra1* mutant strains did not
481 impact the degree of inflammation of the atopic dermatitis-like skin, as assessed by quantification of ear

swelling (**Figures S2A, B**). Together these data demonstrate the importance of *Ms* Rim signaling in fungal survival at alkaline pH, both in vitro as well as in physiologically relevant sites for this commensal microorganism.

Discussion

Malassezia species are among the most common commensal fungi present on the skin, and they are increasingly noted as frequent components of the human gut microbiome [51]. Although most skin sites have a relatively acidic pH, the pH of skin can vary dramatically based on health and disease states. Similar to other fungi, *Malassezia* species possess genes predicted to encode the major components of the pH-responsive Rim signal transduction pathway. We have shown that an intact Rim pathway is required for survival on neutral to alkaline pH as well as elevated salt concentrations, similar to other fungal species. We have also demonstrated that the *M. sympodialis* Rra1 protein is required for fungal survival at alkaline pH, suggesting that Rra1 orthologs are conserved pH-responsive upstream components of Rim signaling in basidiomycetes, likely serving a similar function as the ascomycete Rim21 pH sensors [18]. Finally, we provide evidence that the Rim101/Rra1 pathway increases the fitness of *Malassezia in vivo* in skin exhibiting an elevated pH as it is the case in atopic dermatitis.

Our RNA-Seq analysis of the *M. sympodialis rim101*Δ and *rra1*Δ mutants demonstrated strikingly similar patterns of transcription, further functionally linking *Ms*Rim101 and *Ms*Rra1. Genes demonstrating similar patterns of transcriptional regulation by both Rim101 and Rra1 include those encoding membrane transporters and proteins involved in cell surface adaptation and intracellular trafficking. Proteins involved in similar cell processes are regulated by the Rim101/PacC protein in other fungal species, including the related basidiomycete *C. neoformans* [52]. The fungal cell wall undergoes dramatic changes in structure in response to increases in pH [17] , resulting in enhanced fungal survival in this new environmental condition. Therefore, defects in Rim signaling, and the associated failure of pH-responsive cell wall adaptations, may be a major reason for the alkaline pH growth sensitivity in Rim pathway mutant strains.

We also observed Rim pathway-dependent transcriptional changes in genes involved in membrane lipid biosynthesis. This observation is consistent with recent studies in *C. neoformans* Rim

signaling in which the phospholipid asymmetry and composition of membranes affect Rim pathway activation [52]. More detailed analysis of the *M. sympodialis* transcriptome is limited by the incomplete annotation of the recently assembled *M. sympodialis* genome [25], with many of the genes demonstrating Rim pathway-dependent expression being listed as uncharacterized proteins. However, these data further demonstrate how the fungal-specific Rim/Pal signaling cascade directs adaptive cellular changes to address the unique challenges resulting from alkaline extracellular environments. They also suggest that basidiomycetes and ascomycetes have incorporated structurally related but distinct proteins as pH sensors at the plasma membrane.

Interestingly, Rim101 regulation only accounts for a subset of the genes that are up- or down-regulated in response to alkaline pH. However, a large portion of the genes whose expression appears to be Rim101-dependent overlap with the up- or down-regulated genes in the WT in response to DMEM. Overall, these data suggest that many Rim101-regulated processes are conserved between *M. sympodialis* and other distantly related fungal species.

In many fungal species, mutations in Rim/Pal pathway signaling elements result in a marked attenuation of virulence. For example, *C. albicans* Rim pathway mutants are defective in the yeast-hyphal transition in response to elevation in pH, and they are accordingly avirulent in animal models of infection [53]. Related mutations in the *Aspergillus fumigatus* Pal/PacC pathway display reduced hyphal growth in infected lungs [42]. In the case of *C. neoformans*, Rim pathway mutants are defective in many phenotypes typically associated with pathogenesis in this species: these mutant strains are unable to grow well at mammalian pH, as well as in the presence of iron deprivation. Moreover, *C. neoformans rim* mutants fail to incorporate capsular polysaccharide on the cell surface [10]. Consistent with these *in vitro* observations, *C. neoformans rim* mutants have reduced fungal burdens as assessed by quantitative cultures of infected lungs in animal models of cryptococcosis [10]. Paradoxically, mice infected with these attenuated *rim* mutant strains display decreased survival compared to mice infected with wildtype

strains [10, 18]. This observation has been explained by excessive immunopathology in the *rim* mutant infections. *C. neoformans* Rim pathway mutations result in an unmasking of typically hidden and immunogenic cell wall epitopes, leading to hyperstimulation of innate immune cell activation and accelerated tissue damage [18].

We did not observe Rim pathway-dependent changes in the degree to which *M. sympodialis* activates macrophages *in vitro*. The *Ms* wildtype, *rim101*Δ, and *rra1*Δ strains induced similar levels of TNF production during *in vitro* macrophage/fungal co-culture experiments. However, in contrast to *C. neoformans* in which the wildtype strains effectively suppress macrophage activation, *M. sympodialis* strains display constitutively high levels of macrophage TNF production, similar to *C. albicans*. Therefore, *M. sympodialis*, though a common commensal, does not appear to shield itself from immune recognition as efficiently as encapsulated fungi such as *C. neoformans*. To fully understand the role of the Rim/Pal1 pathway in the antifungal response to *Malassezia*, future studies with skin-resident cells and model systems harboring features characteristic of the cutaneous niche will be needed.

Emerging data from microbiome studies suggest that *Malassezia* species are not only common skin colonizers but are also found in the human gut, where the pH varies widely from very acidic in the stomach to more alkaline in the small and large intestines. The presence of *Malassezia* species in these micro-niches has been associated with longer term sequelae of continuous antigenic stimulation, including inflammatory bowel disease [54]. Further exploration of the interaction of this commensal fungus with the immune system may elucidate ways in which *Malassezia* species might contribute to health or disease at specific anatomic sites.

Acknowledgements

This work was supported by NIH grants AI074677 and AI175711 (JAA), F31A140427 (HEB), 1R21AI168672-01A1 (JH and SLL), a National Defense Science and Engineering Grant to KMP awarded by the US Department of Defense (Office of Scientific Research, 32 CFR 168a) and a Swiss National Science Foundation grant to SLL (310030_189255). RNA-Seq studies were supported by a Pilot Grant from the Duke University School of Medicine to support Shared Resource Facilities (Duke Sequencing and Genomic technologies Shared Resource). KMP was supported by a Duke University Bass Instructional Fellowship. Scanning electron microscopy was performed in part at the Chapel Hill Analytical and Nanofabrication Laboratory, CHANL, a member of the North Carolina Research Triangle Nanotechnology Network, RTNN, which is supported by the National Science Foundation, Grant ECCS-1542015, as part of the National Nanotechnology Coordinated Infrastructure, NNCI. We would like to thank Fiorella Ruchti for establishing the experimental conditions for the *in vivo* experiments.

Author Contributions

KMP, SLL, JH, GI, and JAA were involved with the conception and design of experiments. KMP, CLT, HEB, JTB, EGI, and GI were involved in direct experimentation and acquisition of the data. All authors participated in the analysis and interpretation of the data, as well as in the writing process.

Table 1. Functional categories enriched among the genes differentially expressed in DMEM in both the *rim101*Δ and *rra1*Δ mutant strains. Functional category assignment was performed manually based on predicted gene function using FungiDB annotations (2022).

Functional category	Gene ID	Gene name	Predicted protein function
Upregulated			
Membrane transport	MSYG_3909	*ATO2*	Putative transmembrane protein involved in export of ammonia
	MSYG_2629		MFS domain-containing protein
	MSYG_3908		MFS domain-containing protein
	MSYG_3150	*FCY21*	Putative purine-cytosine permease
	MSYG_0038		MFS domain-containing protein
	MSYG_4234	*FCY2*	Purine-cytosine permease
	MSYG_0981		MFS domain-containing protein
	MSYG_4142	*SPA2*	Component of the polarisome
	MSYG_3302		MFS domain-containing protein
Cell cycle regulation	MSYG_1748		Csm1 domain-containing protein
	MSYG_1957	*PXL1*	Protein that localizes to sites of polarized growth
	MSYG_0194		Cyclin N-terminal domain-containing protein
	MSYG_0335		SH3 domain-containing protein
	MSYG_2712		Cyclin N-terminal domain-containing protein
Cell surface modifications	MSYG_4357		Chitin deacetylase
	MSYG_1041		Glyco trans 2-like domain-containing protein
Downregulated			
Protein synthesis	MSYG_1555		Prolyl-tRNA synthetase
	MSYG_0269		tRNA-dihydrouridine synthase
	MSYG_4576		tRNA-Glu
	MSYG_4544		tRNA-Glu
Cell cycle regulation	MSYG_0270		Spc7 domain-containing protein
	MSYG_1674		SRR1 domain-containing protein
	MSYG_1379		CRAL-TRIO domain-containing protein
Cell surface modifications	MSYG_0176		Mannose-P-dolichol utilization defect 1 protein homolog
	MSYG_1904	*ROT1*	Protein chaperone
	MSYG_1333		alpha-1,2-Mannosidase
Intracellular trafficking	MSYG_3869		Vps8 domain-containing protein
	MSYG_2318		Adaptin N domain-containing protein
	MSYG_2610	*TRS33*	Core component of transport protein particle (TRAPP) complex
Lipid metabolism	MSYG_1989		Fatty acid hydroxylase domain-containing protein
	MSYG_0629	*ERG5*	C-22 sterol desaturase

576 **Table 2**. Functional categories enriched among the genes differentially expressed in the presence of alkaline pH
577 (pH 7.5) in both the *rim101*Δ and *rra1*Δ mutant strains. Functional category assignment was performed manually
578 based on predicted gene function using FungiDB annotations (2022).
579
580

Functional category	Gene ID	Gene name	Predicted protein function
Upregulated			
Membrane transport	MSYG_0981		MFS domain-containing protein
	MSYG_3302		MFS domain-containing protein
	MSYG_0839		AA permease domain-containing protein
	MSYG_2629		MFS domain-containing protein
	MSYG_3150	*FCY1*	Putative purine-cytosine permease
Redox metabolism	MSYG_3153		L-ornithine N(5)-monooxygenase
	MSYG_4146		NMO domain-containing protein
	MSYG_4103	*CYB2*	Cytochrome b2 (L-lactate cytochrome-c oxidoreductase)
	MSYG_0029		Aldedh domain-containing protein
Intracellular transport	MSYG_0982	*YPT31*	Rab family GTPase
	MSYG_3478		CRAL-TRIO domain-containing protein
	MSYG_1774	*VPS25*	Component of the ESCRT-II complex
Fatty acid metabolism	MSYG_1824		SCP2 domain-containing protein
	MSYG_3126		Lipase 3 domain-containing protein
Downregulated			
Membrane transport	MSYG_1125		Ammonium transporter
	MSYG_1634	*MUP1*	Cation ATPase N domain-containing protein
	MSYG_3059		High affinity methionine permease
	MSYG_3009		Na H Exchanger domain-containing protein
	MSYG_3517		MFS domain-containing protein
Redox metabolism	MSYG_1484		GMC OxRdtase N domain-containing protein

581
582

583 **Figure Legends**

584 **Figure 1**. (A) ***M. sympodialis RIM101*** **and** ***RRA1*** **genes are required for optimal growth at alkaline pH**
585 **and in high salt conditions**. Indicated strains were serially diluted and incubated in spot cultures on
586 mDixon medium buffered to pH 6, pH 7, or pH 7.5, or mDixon medium supplemented with 1 M NaCl to
587 examine growth phenotypes. Plates were imaged 6 days post-inoculation. (B) ***M. sympodialis RIM101***
588 **gene expression in response to increasing pH and tissue culture medium.** Wild-type *M. sympodialis*
589 cells were incubated overnight in mDixon medium pH 4, then shifted to one of the following conditions
590 for 90 minutes: mDixon buffered to pH 4, pH 6, pH 7, pH 7.25, or pH 7.5; or tissue culture medium
591 (DMEM or RPMI + 10% FBS). Relative transcript abundance of the *RIM101* gene was assessed by
592 quantitative real-time PCR using the $\Delta\Delta C_T$ method and the *TUB2* tubulin gene as control. Fold-change
593 values for each condition were normalized to mDixon pH 4.
594
595 **Figure 2. Comparative transcriptional analysis.** The *M. sympodialis* WT, *rim101*Δ, and *rra1*Δ strains
596 were incubated in each of the following conditions for 90 minutes prior to total RNA extraction for
597 RNAseq analysis: mDixon medium pH 4, mDixon medium pH 7.5, DMEM. (**A**) Comparison of global
598 transcriptome patterns by Multidimensional Scaling (MDS) analysis (3 biological replicates for each
599 indicated strain in each condition). (**B**) Volcano plots illustrating number of genes with statistically
600 significant alterations in transcript abundance at pH 7.5 and pH4. Genes with alterations in transcript
601 abundance (+/- 1 $\log_2$ fold change) are indicated in green (*rim101*Δ versus WT) or magenta (*rra1*Δ versus
602 WT). (**C**) Venn diagram indicating the number of genes with statistically significant differences in
603 transcript abundance (+/- 1 $\log_2$ fold change) for indicated strains compared to WT at pH 7.5 (green =
604 *rim101*Δ, magenta = *rra1*Δ). (**D**) Venn diagram indicating the number of genes with statistically
605 significant differences in transcript abundance (+/- 1 $\log_2$ fold change) for indicated strains compared to
606 WT in DMEM (green = *rim101*Δ, magenta = *rra1*Δ).

Figure 3. *M. sympodialis* interactions with macrophages. (**A**) Light microscopy image of the WT strain co-cultured with J774A.1 macrophages after one hour of co-culture. (**B**) The WT strain, *rim101*Δ mutant strains, and *rra1*Δ mutant strains were co-incubated with (left) and without (right) J774A.1 murine macrophages for 4 hours. Survival of the indicated fungal strains was assessed by quantitative culture, and the percentage of recovered (output) colony forming units (CFUs) compared to the original (input) CFUs was normalized to the WT strain [% WT (output/input)]. This experiment was performed with a minimum of three biological replicates (n = 3). Error bars represent the SEM compared to WT. Log transformation was used to normally distribute the data for statistical analysis (one-way ANOVA; ns, not significant). (**C**) Scanning electron microscopy (SEM) images of the WT strain, the *rim101*Δ mutant strain (KPY34), and the *rra1*Δ mutant strain (KPY38) after one hour of co-culture with J774A.1 macrophages. Cells were fixed with 2.5% glutaraldehyde, dehydrated, critical point dried, sputter-coated with gold-palladium, and imaged. Red arrowheads indicate fungal cells actively undergoing macrophage phagocytosis. Yellow arrowheads indicate potential macrophage extracellular traps (METs).

Figure 4. *M. sympodialis* elicits TNF response when co-cultured with macrophages

The *M. sympodialis* WT, *rim101*Δ, and *rra1*Δ strains were incubated for 3 days in DMEM + 10% FBS at 30°C preceding a final incubation at 37°C for 16 hours prior to co-culture. WT *C. neoformans* (strain H99) cells were incubated for 2 days in DMEM + 10% FBS at 30°C preceding a final incubation at 37°C for 16 hours prior to co-culture. WT *C. albicans* (SC5314) cells were incubated for 1 day in DMEM without serum at 30°C prior to co-culture. Bone marrow-derived macrophages (BMMs) were co-incubated with the indicated fungal strains for 3 hours (**A**) or 6 hours (**B**) at a multiplicity of infection (MOI) of 10:1, fungal cells:BMMs. TNF levels (pg/ml) were assayed from the co-culture supernatant by ELISA. Data represent means from 6 replicates per strain per condition. One-way ANOVA and Tukey's multiple

comparison test were used to compare means. ****, $p < 0.0001$; ***, $p < 0.001$; *, $p = 0.0186$. Statistical comparisons were made against WT *M. sympodialis*.

Figure 5. The Rim/Pal1 pathway impacts *M. sympodialis* fitness in a murine model of atopic dermatitis.

The ear skin of WT C57BL/6 mice was repeatedly treated with either an ethanol solvent control (low pH, panel A) or with MC903 (high pH, panels A and B) for 10 days to induce an atopic dermatitis-like state. Treated skin was then associated dorsally with *M. sympodialis* WT, *rim101*Δ [KPY34] and *rra1*Δ [KPY36]. The skin fungal load was quantified after 4 days (**A**) or 7 days (**B**) of colonization. Each symbol represents one animal. The mean of each group is indicated (dotted line, detection limit). Two-way ANOVA (**A**) or One-way ANOVA (**B**) were used to determine the statistical significance of the mean colony-forming units (cfu) of each mutant against WT *M. sympodialis*. *, $p < 0.05$.

Supplemental Figure Legends

Figure S1. Correlation of gene expression in the *rim101*Δ and *rra1*Δ strains. The *Ms* WT, *rim101*Δ, and *rra1*Δ strains were incubated for 90 minutes in mDixon medium pH 4, mDixon medium pH 7.5, or DMEM tissue culture medium (pH 7.4). Deep RNA sequencing was performed for each strain at each condition, and the $\log_2$ fold-change for each gene was calculated for the *rim101*Δ and *rra1*Δ strains compared to the WT strain. Gene expression is highly correlated between *rim101*Δ and *rra1*Δ mutants at pH 7.5 and in DMEM, but not at pH 4. Red points indicate genes with expression in *rim101*Δ and *rra1*Δ that is significantly different from WT (adjusted p-value <= 0.05).

Figure S2. *M. sympodialis* TNF induction is not dependent on fungal cell viability. WT, *rim101*Δ (KPY34), and *rra1*Δ (KPY36) *M. sympodialis* mutant strains were incubated for 3 days in DMEM + 10%

FBS and PenStrep at 30°C preceding a final incubation at 37°C for 16 hours prior to co-culture. WT (H99) *C. neoformans* cells were incubated for 2 days in DMEM + 10% FBS and PenStrep at 30°C preceding a final incubation at 37°C for 16 hours prior to co-culture. WT *C. albicans* (SC5314) cells were incubated for 1 day in DMEM without serum at 30°C prior to co-culture. Bone marrow-derived macrophages (BMMs) were co-incubated for 3 hours with heat-killed (HK) fungal cells (HK, 1 hour at 65°C). BMMs were co-incubated with fungal cells for 6 hours following a 3-hour LPS priming. All strains were at a multiplicity of infection (MOI) of 10:1, fungal cells : BMMs. TNF levels (pg/ml) were assayed from the co-culture supernatant by ELISA. Data represent means from 6 replicates per strain per condition. One-way ANOVA and Tukey's multiple comparison test were used to compare means. ****, $p < 0.0001$; *, $p < 0.006$. Statistical comparisons were made against WT *M. sympodialis*.

Figure S3. The *M. sympodialis* Rim101/Rra1 pathway does not impact inflammation in a murine model of atopic dermatitis. To simulate high and low pH under *in vivo* conditions, the ear skin of WT C57BL/6 mice was treated with MC903 (high pH) or EtOH (solvent control, low pH) and then associated with *M. sympodialis* WT, *rim101*Δ [KPY34] and *rra1*Δ [KPY36]. The treatment schedule is indicated at the top of the graph with solid arrows indicating dorsal and ventral application of MC903 or EtOH, and dashed arrows indicate ventral application only of MC903 or EtOH. The ear thickness of mice was determined at the indicated time points. Each datapoint is the mean +/- SD of 4 (**A**) or 5 mice (**B**), respectively.

References

1. Ali SM, Yosipovitch G. Skin pH: from basic science to basic skin care. Acta Derm Venereol. 2013;93(3):261-7. doi: 10.2340/00015555-1531. PubMed PMID: 23322028.
2. Selander C, Zargari A, Mollby R, Rasool O, Scheynius A. Higher pH level, corresponding to that on the skin of patients with atopic eczema, stimulates the release of Malassezia sympodialis allergens. Allergy. 2006;61(8):1002-8. doi: 10.1111/j.1398-9995.2006.01108.x. PubMed PMID: 16867055.
3. Aykut B, Pushalkar S, Chen R, Li Q, Abengozar R, Kim JI, et al. The fungal mycobiome promotes pancreatic oncogenesis via activation of MBL. Nature. 2019;574(7777):264-7. Epub 20191002. doi: 10.1038/s41586-019-1608-2. PubMed PMID: 31578522; PubMed Central PMCID: PMCPMC6858566.
4. Selvig K, Alspaugh JA. pH Response Pathways in Fungi: Adapting to Host-derived and Environmental Signals. Mycobiology. 2011;39(4):249-56. doi: 10.5941/MYCO.2011.39.4.249. PubMed PMID: 22783112; PubMed Central PMCID: PMCPMC3385132.
5. Cornet M, Gaillardin C. pH signaling in human fungal pathogens: a new target for antifungal strategies. Eukaryot Cell. 2014;13(3):342-52. Epub 20140117. doi: 10.1128/EC.00313-13. PubMed PMID: 24442891; PubMed Central PMCID: PMCPMC3957587.
6. Penalva MA, Tilburn J, Bignell E, Arst HN, Jr. Ambient pH gene regulation in fungi: making connections. Trends Microbiol. 2008;16(6):291-300. Epub 20080503. doi: 10.1016/j.tim.2008.03.006. PubMed PMID: 18457952.
7. Obara K, Yamamoto H, Kihara A. Membrane protein Rim21 plays a central role in sensing ambient pH in Saccharomyces cerevisiae. The Journal of biological chemistry. 2012;287(46):38473-81. Epub 20120927. doi: 10.1074/jbc.M112.394205. PubMed PMID: 23019326; PubMed Central PMCID: PMCPMC3493892.
8. Arst HN, Jr., Bignell E, Tilburn J. Two new genes involved in signalling ambient pH in Aspergillus nidulans. Mol Gen Genet. 1994;245(6):787-90. doi: 10.1007/BF00297286. PubMed PMID: 7830727.
9. Treton B, Blanchin-Roland S, Lambert M, Lepingle A, Gaillardin C. Ambient pH signalling in ascomycetous yeasts involves homologues of the Aspergillus nidulans genes palF and paIH. Mol Gen Genet. 2000;263(3):505-13. doi: 10.1007/s004380051195. PubMed PMID: 10821185.
10. O'Meara TR, Norton D, Price MS, Hay C, Clements MF, Nichols CB, Alspaugh JA. Interaction of Cryptococcus neoformans Rim101 and protein kinase A regulates capsule. PLoS pathogens. 2010;6(2):e1000776. PubMed PMID: 20174553.
11. Li W, Mitchell AP. Proteolytic activation of Rim1p, a positive regulator of yeast sporulation and invasive growth. Genetics. 1997;145(1):63-73. doi: 10.1093/genetics/145.1.63. PubMed PMID: 9017390; PubMed Central PMCID: PMCPMC1207785.
12. Diez E, Alvaro J, Espeso EA, Rainbow L, Suarez T, Tilburn J, et al. Activation of the Aspergillus PacC zinc finger transcription factor requires two proteolytic steps. The EMBO journal. 2002;21(6):1350-9. doi: 10.1093/emboj/21.6.1350. PubMed PMID: 11889040; PubMed Central PMCID: PMCPMC125927.
13. Tilburn J, Sarkar S, Widdick DA, Espeso EA, Orejas M, Mungroo J, et al. The Aspergillus PacC zinc finger transcription factor mediates regulation of both acid- and alkaline-

718 expressed genes by ambient pH. The EMBO journal. 1995;14(4):779-90. doi: 10.1002/j.1460-
719 2075.1995.tb07056.x. PubMed PMID: 7882981; PubMed Central PMCID: PMCPMC398143.
720 14. O'Meara TR, Xu W, Selvig KM, O'Meara MJ, Mitchell AP, Alspaugh JA. The
721 Cryptococcus neoformans Rim101 transcription factor directly regulates genes required for
722 adaptation to the host. Molecular and cellular biology. 2014;34(4):673-84. doi:
723 10.1128/MCB.01359-13. PubMed PMID: 24324006; PubMed Central PMCID: PMC3911494.
724 15. Cornet M, Bidard F, Schwarz P, Da Costa G, Blanchin-Roland S, Dromer F, Gaillardin
725 C. Deletions of endocytic components VPS28 and VPS32 affect growth at alkaline pH and
726 virulence through both RIM101-dependent and RIM101-independent pathways in Candida
727 albicans. Infection and immunity. 2005;73(12):7977-87. doi: 10.1128/IAI.73.12.7977-
728 7987.2005. PubMed PMID: 16299290; PubMed Central PMCID: PMCPMC1307034.
729 16. Garnaud C, Garcia-Oliver E, Wang Y, Maubon D, Bailly S, Despinasse Q, et al. The Rim
730 Pathway Mediates Antifungal Tolerance in Candida albicans through Newly Identified Rim101
731 Transcriptional Targets, Including Hsp90 and Ipt1. Antimicrobial agents and chemotherapy.
732 2018;62(3). Epub 20180223. doi: 10.1128/AAC.01785-17. PubMed PMID: 29311085; PubMed
733 Central PMCID: PMCPMC5826160.
734 17. O'Meara TR, Holmer SM, Selvig K, Dietrich F, Alspaugh JA. Cryptococcus neoformans
735 Rim101 is associated with cell wall remodeling and evasion of the host immune responses.
736 MBio. 2013;4(1). doi: 10.1128/mBio.00522-12. PubMed PMID: 23322637; PubMed Central
737 PMCID: PMC3551547.
738 18. Ost KS, O'Meara TR, Huda N, Esher SK, Alspaugh JA. The Cryptococcus neoformans
739 alkaline response pathway: identification of a novel rim pathway activator. PLoS Genet.
740 2015;11(4):e1005159. doi: 10.1371/journal.pgen.1005159. PubMed PMID: 25859664; PubMed
741 Central PMCID: PMC4393102.
742 19. Cervantes-Chavez JA, Ortiz-Castellanos L, Tejeda-Sartorius M, Gold S, Ruiz-Herrera J.
743 Functional analysis of the pH responsive pathway Pal/Rim in the phytopathogenic basidiomycete
744 Ustilago maydis. Fungal Genet Biol. 2010;47(5):446-57. doi: 10.1016/j.fgb.2010.02.004.
745 PubMed PMID: 20153837.
746 20. Arechiga-Carvajal ET, Ruiz-Herrera J. The RIM101/pacC homologue from the
747 basidiomycete Ustilago maydis is functional in multiple pH-sensitive phenomena. Eukaryot Cell.
748 2005;4(6):999-1008. doi: 10.1128/EC.4.6.999-1008.2005. PubMed PMID: 15947192; PubMed
749 Central PMCID: PMCPMC1151993.
750 21. Pianalto KM, Ost KS, Brown HE, Alspaugh JA. Characterization of additional
751 components of the environmental pH-sensing complex in the pathogenic fungus Cryptococcus
752 neoformans. The Journal of biological chemistry. 2018;293(26):9995-10008. Epub 2018/05/18.
753 doi: 10.1074/jbc.RA118.002741. PubMed PMID: 29769315; PubMed Central PMCID:
754 PMCPMC6028953.
755 22. Wu G, Zhao H, Li C, Rajapakse MP, Wong WC, Xu J, et al. Genus-Wide Comparative
756 Genomics of Malassezia Delineates Its Phylogeny, Physiology, and Niche Adaptation on Human
757 Skin. PLoS Genet. 2015;11(11):e1005614. Epub 20151105. doi: 10.1371/journal.pgen.1005614.
758 PubMed PMID: 26539826; PubMed Central PMCID: PMCPMC4634964.
759 23. Ianiri G, Applen Clancey S, Lee SC, Heitman J. FKBP12-Dependent Inhibition of
760 Calcineurin Mediates Immunosuppressive Antifungal Drug Action in Malassezia. MBio.
761 2017;8(5). Epub 2017/10/27. doi: 10.1128/mBio.01752-17. PubMed PMID: 29066552; PubMed
762 Central PMCID: PMCPMC5654937.

763 24. Sparber F, De Gregorio C, Steckholzer S, Ferreira FM, Dolowschiak T, Ruchti F, et al.
764 The Skin Commensal Yeast Malassezia Triggers a Type 17 Response that Coordinates Anti-
765 fungal Immunity and Exacerbates Skin Inflammation. Cell host & microbe. 2019;25(3):389-403
766 e6. doi: 10.1016/j.chom.2019.02.002. PubMed PMID: 30870621.
767 25. Zhu Y, Engstrom PG, Tellgren-Roth C, Baudo CD, Kennell JC, Sun S, et al.
768 Proteogenomics produces comprehensive and highly accurate protein-coding gene annotation in
769 a complete genome assembly of Malassezia sympodialis. Nucleic acids research.
770 2017;45(5):2629-43. doi: 10.1093/nar/gkx006. PubMed PMID: 28100699; PubMed Central
771 PMCID: PMCPMC5389616.
772 26. Ianiri G, Boyce KJ, Idnurm A. Isolation of conditional mutations in genes essential for
773 viability of Cryptococcus neoformans. Current genetics. 2017;63(3):519-30. Epub 20161025.
774 doi: 10.1007/s00294-016-0659-2. PubMed PMID: 27783209; PubMed Central PMCID:
775 PMCPMC5405016.
776 27. Ianiri G, Averette AF, Kingsbury JM, Heitman J, Idnurm A. Gene Function Analysis in
777 the Ubiquitous Human Commensal and Pathogen Malassezia Genus. MBio. 2016;7(6). Epub
778 20161129. doi: 10.1128/mBio.01853-16. PubMed PMID: 27899504; PubMed Central PMCID:
779 PMCPMC5137500.
780 28. Dobin A, Davis CA, Schlesinger F, Drenkow J, Zaleski C, Jha S, et al. STAR: ultrafast
781 universal RNA-seq aligner. Bioinformatics. 2013;29(1):15-21. Epub 2012/10/30. doi:
782 10.1093/bioinformatics/bts635. PubMed PMID: 23104886; PubMed Central PMCID:
783 PMCPMC3530905.
784 29. Love MI, Anders S, Kim V, Huber W. RNA-Seq workflow: gene-level exploratory
785 analysis and differential expression. F1000Res. 2015;4:1070. Epub 2015/12/18. doi:
786 10.12688/f1000research.7035.1. PubMed PMID: 26674615; PubMed Central PMCID:
787 PMCPMC4670015.
788 30. Love MI, Huber W, Anders S. Moderated estimation of fold change and dispersion for
789 RNA-seq data with DESeq2. Genome Biol. 2014;15(12):550. Epub 2014/12/18. doi:
790 10.1186/s13059-014-0550-8. PubMed PMID: 25516281; PubMed Central PMCID:
791 PMCPMC4302049.
792 31. Alvarez-Jarreta J, Amos B, Aurrecoechea C, Bah S, Barba M, Barreto A, et al.
793 VEuPathDB: the eukaryotic pathogen, vector and host bioinformatics resource center in 2023.
794 Nucleic acids research. 2024;52(D1):D808-D16. doi: 10.1093/nar/gkad1003. PubMed PMID:
795 37953350; PubMed Central PMCID: PMCPMC10767879.
796 32. Esher SK, Ost KS, Kozubowski L, Yang DH, Kim MS, Bahn YS, et al. Relative
797 Contributions of Prenylation and Postprenylation Processing in Cryptococcus neoformans
798 Pathogenesis. mSphere. 2016;1(2). doi: 10.1128/mSphere.00084-15. PubMed PMID: 27303728;
799 PubMed Central PMCID: PMCPMC4894686.
800 33. Ianiri G, Coelho MA, Ruchti F, Sparber F, McMahon TJ, Fu C, et al. HGT in the human
801 and skin commensal Malassezia: A bacterially derived flavohemoglobin is required for NO
802 resistance and host interaction. Proc Natl Acad Sci U S A. 2020;117(27):15884-94. Epub
803 20200623. doi: 10.1073/pnas.2003473117. PubMed PMID: 32576698; PubMed Central PMCID:
804 PMCPMC7354939.
805 34. Ost KS, Esher SK, Leopold Wager CM, Walker L, Wagener J, Munro C, et al. Rim
806 Pathway-Mediated Alterations in the Fungal Cell Wall Influence Immune Recognition and
807 Inflammation. MBio. 2017;8(1). doi: 10.1128/mBio.02290-16. PubMed PMID: 28143983;
808 PubMed Central PMCID: PMCPMC5285508.

809 35. Esher SK, Ost KS, Kohlbrenner MA, Pianalto KM, Telzrow CL, Campuzano A, et al.
810 Defects in intracellular trafficking of fungal cell wall synthases lead to aberrant host immune
811 recognition. PLoS pathogens. 2018;14(6):e1007126. Epub 2018/06/05. doi:
812 10.1371/journal.ppat.1007126. PubMed PMID: 29864141; PubMed Central PMCID:
813 PMCPMC6002136.
814 36. Russell WM. The development of the three Rs concept. Altern Lab Anim.
815 1995;23(3):298-304. PubMed PMID: 11656565.
816 37. Moosbrugger-Martinz V, Schmuth M, Dubrac S. A Mouse Model for Atopic Dermatitis
817 Using Topical Application of Vitamin D3 or of Its Analog MC903. Methods Mol Biol.
818 2017;1559:91-106. doi: 10.1007/978-1-4939-6786-5_8. PubMed PMID: 28063040.
819 38. Ruchti F, Zwicky P, Becher B, Dubrac S, LeibundGut-Landmann S. Epidermal barrier
820 impairment predisposes for excessive growth of the allergy-associated yeast Malassezia on
821 murine skin. Allergy. 2024. Epub 20240222. doi: 10.1111/all.16062. PubMed PMID: 38385963.
822 39. Xie L, McKenzie CI, Qu X, Mu Y, Wang Q, Bing N, et al. pH and Proton Sensor GPR65
823 Determine Susceptibility to Atopic Dermatitis. J Immunol. 2021;207(1):101-9. Epub 20210616.
824 doi: 10.4049/jimmunol.2001363. PubMed PMID: 34135065; PubMed Central PMCID:
825 PMCPMC8674371.
826 40. Sparber F, LeibundGut-Landmann S. Infecting Mice with Malassezia spp. to Study the
827 Fungus-Host Interaction. J Vis Exp. 2019;(153). Epub 20191106. doi: 10.3791/60175. PubMed
828 PMID: 31762452.
829 41. Bignell E, Negrete-Urtasun S, Calcagno AM, Haynes K, Arst HN, Jr., Rogers T. The
830 Aspergillus pH-responsive transcription factor PacC regulates virulence. Mol Microbiol.
831 2005;55(4):1072-84. doi: 10.1111/j.1365-2958.2004.04472.x. PubMed PMID: 15686555.
832 42. Bertuzzi M, Schrettl M, Alcazar-Fuoli L, Cairns TC, Munoz A, Walker LA, et al. The
833 pH-responsive PacC transcription factor of Aspergillus fumigatus governs epithelial entry and
834 tissue invasion during pulmonary aspergillosis. PLoS pathogens. 2014;10(10):e1004413. doi:
835 10.1371/journal.ppat.1004413. PubMed PMID: 25329394; PubMed Central PMCID:
836 PMC4199764.
837 43. Porta A, Ramon AM, Fonzi WA. PRR1, a homolog of Aspergillus nidulans palF, controls
838 pH-dependent gene expression and filamentation in Candida albicans. Journal of bacteriology.
839 1999;181(24):7516-23. doi: 10.1128/JB.181.24.7516-7523.1999. PubMed PMID: 10601209;
840 PubMed Central PMCID: PMCPMC94209.
841 44. Ramon AM, Porta A, Fonzi WA. Effect of environmental pH on morphological
842 development of Candida albicans is mediated via the PacC-related transcription factor encoded
843 by PRR2. Journal of bacteriology. 1999;181(24):7524-30. doi: 10.1128/JB.181.24.7524-
844 7530.1999. PubMed PMID: 10601210; PubMed Central PMCID: PMCPMC94210.
845 45. Brown HE, Telzrow CL, Saelens JW, Fernandes L, Alspaugh JA. Sterol-Response
846 Pathways Mediate Alkaline Survival in Diverse Fungi. MBio. 2020;11(3). Epub 2020/06/18. doi:
847 10.1128/mBio.00719-20. PubMed PMID: 32546619; PubMed Central PMCID:
848 PMCPMC7298709.
849 46. Doster RS, Rogers LM, Gaddy JA, Aronoff DM. Macrophage Extracellular Traps: A
850 Scoping Review. J Innate Immun. 2018;10(1):3-13. Epub 20171007. doi: 10.1159/000480373.
851 PubMed PMID: 28988241; PubMed Central PMCID: PMCPMC6757166.
852 47. Kesavan S, Walters CE, Holland KT, Ingham E. The effects of Malassezia on pro-
853 inflammatory cytokine production by human peripheral blood mononuclear cells in vitro. Med
854 Mycol. 1998;36(2):97-106. PubMed PMID: 9776820.

855 48. Kesavan S, Holland KT, Ingham E. The effects of lipid extraction on the
856 immunomodulatory activity of Malassezia species in vitro. Med Mycol. 2000;38(3):239-47. doi:
857 10.1080/mmy.38.3.239.247. PubMed PMID: 10892993.
858 49. Ashbee HR, Evans EG. Immunology of diseases associated with Malassezia species.
859 Clinical microbiology reviews. 2002;15(1):21-57. doi: 10.1128/CMR.15.1.21-57.2002. PubMed
860 PMID: 11781265; PubMed Central PMCID: PMCPMC118058.
861 50. Jeremias J, Kalo-Klein A, Witkin SS. Individual differences in tumour necrosis factor
862 and interleukin-1 production induced by viable and heat-killed Candida albicans. J Med Vet
863 Mycol. 1991;29(3):157-63. doi: 10.1080/02681219180000261. PubMed PMID: 1890562.
864 51. Scheynius A, Johansson C, Buentke E, Zargari A, Linder MT. Atopic eczema/dermatitis
865 syndrome and Malassezia. Int Arch Allergy Immunol. 2002;127(3):161-9. doi:
866 10.1159/000053860. PubMed PMID: 11979041.
867 52. Brown HE, Ost KS, Esher SK, Pianalto KM, Saelens JW, Guan Z, Andrew Alspaugh J.
868 Identifying a novel connection between the fungal plasma membrane and pH-sensing. Mol
869 Microbiol. 2018;109(4):474-93. Epub 2018/06/10. doi: 10.1111/mmi.13998. PubMed PMID:
870 29885030; PubMed Central PMCID: PMCPMC6173979.
871 53. Davis D. Adaptation to environmental pH in Candida albicans and its relation to
872 pathogenesis. Current genetics. 2003;44(1):1-7. PubMed PMID: 12819929.
873 54. Limon JJ, Tang J, Li D, Wolf AJ, Michelsen KS, Funari V, et al. Malassezia Is
874 Associated with Crohn's Disease and Exacerbates Colitis in Mouse Models. Cell host & microbe.
875 2019;25(3):377-88 e6. Epub 20190305. doi: 10.1016/j.chom.2019.01.007. PubMed PMID:
876 30850233; PubMed Central PMCID: PMCPMC6417942.
877

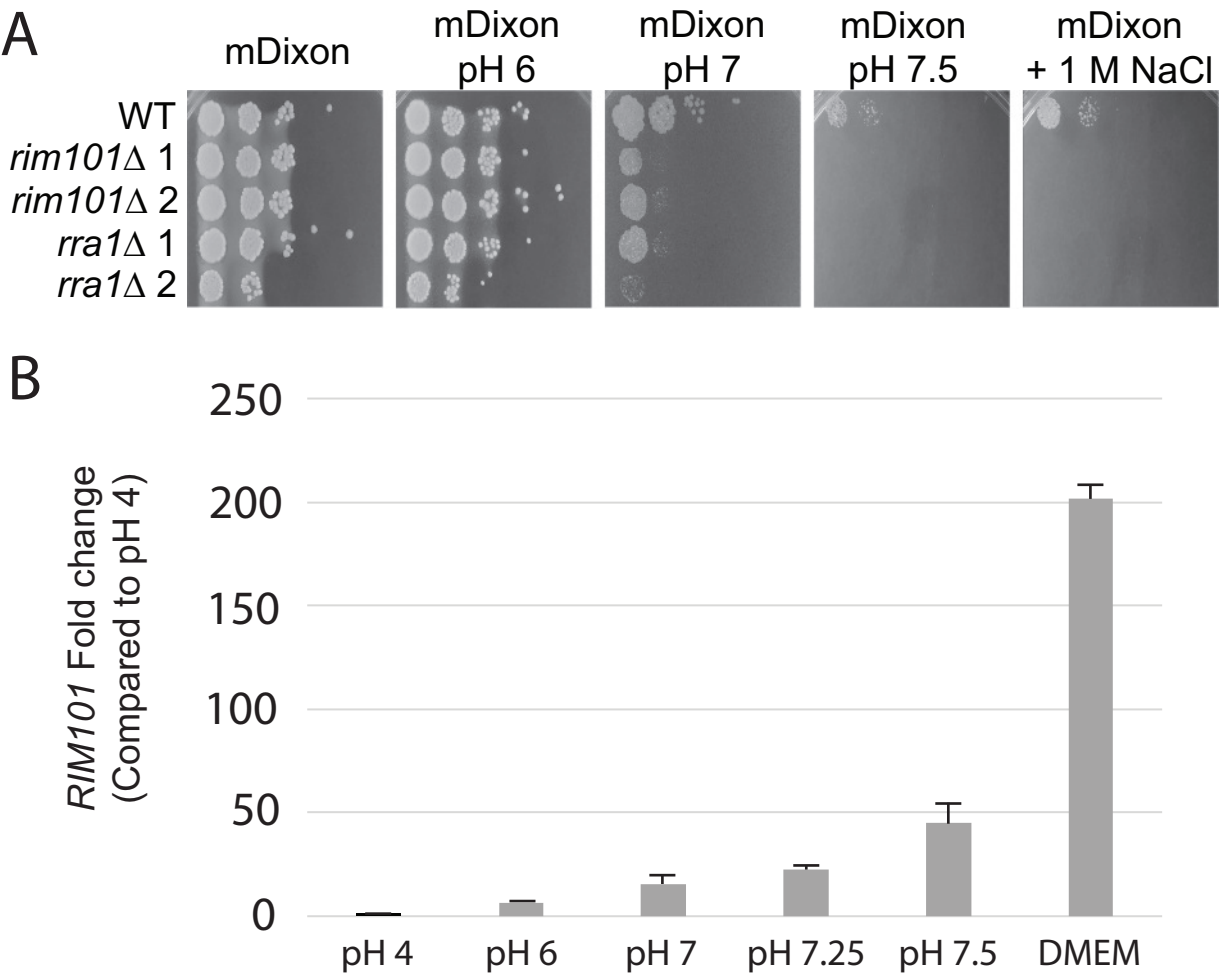
A
mDixon
mDixon pH 6
mDixon pH 7
mDixon pH 7.5
mDixon + 1 M NaCl
WT
rim101Δ 1
rim101Δ 2
rra1Δ 1
rra1Δ 2
B
RIM101 Fold change (Compared to pH 4)
250
200
150
100
50
0
pH 4
pH 6
pH 7
pH 7.25
pH 7.5
DMEM

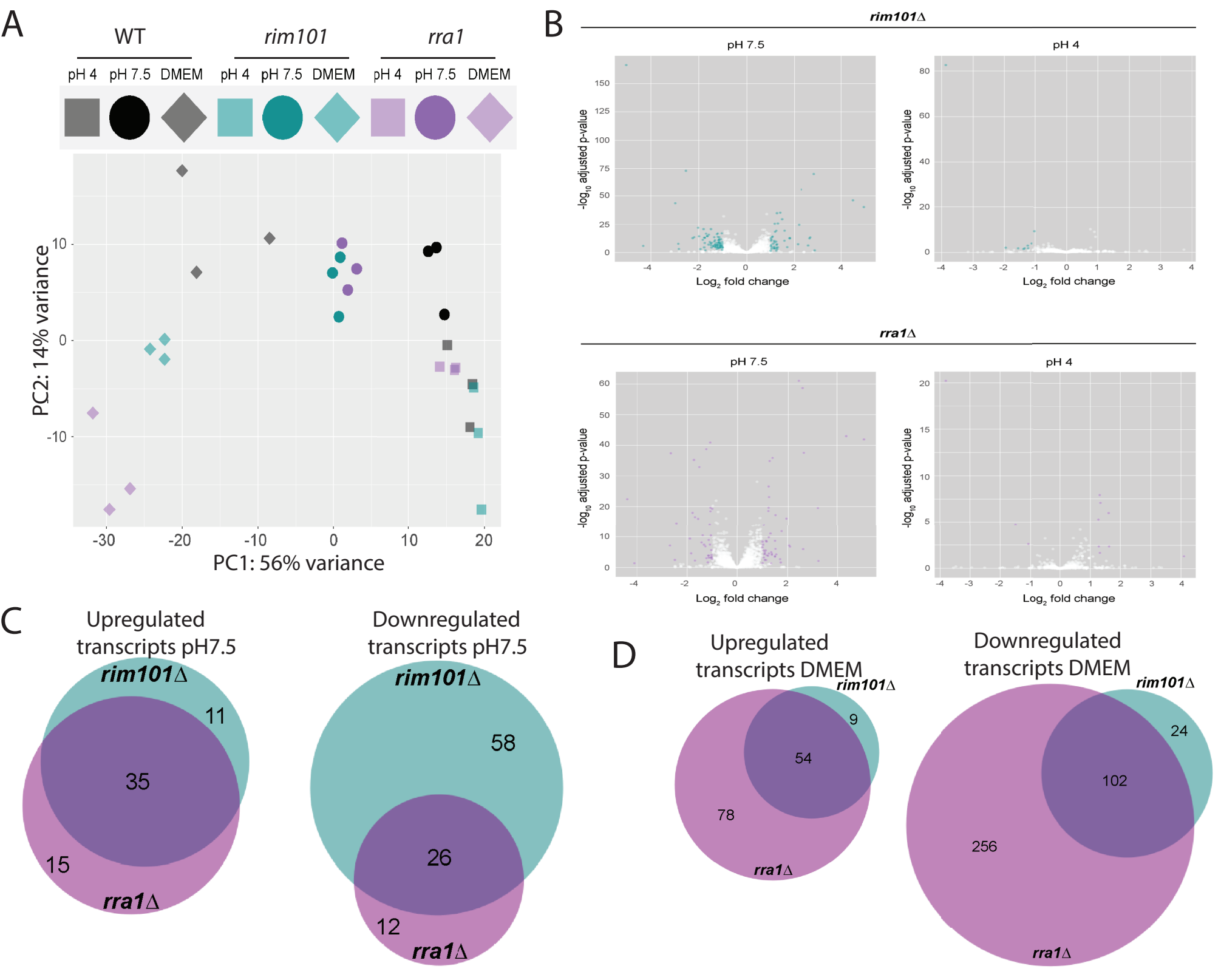
A
WT
rim101
rra1
pH 4
pH 7.5
DMEM
PC2: 14% variance
PC1: 56% variance
B
rim101Δ
rra1Δ
pH 7.5
pH 4
-log10 adjusted p-value
Log2 fold change
C
Upregulated transcripts pH7.5
Downregulated transcripts pH7.5
rim101Δ
rra1Δ
11
35
15
58
26
12
D
Upregulated transcripts DMEM
Downregulated transcripts DMEM
9
54
78
24
102
256

A

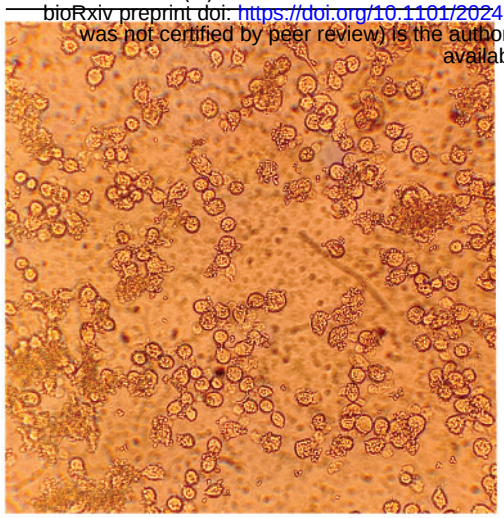

C

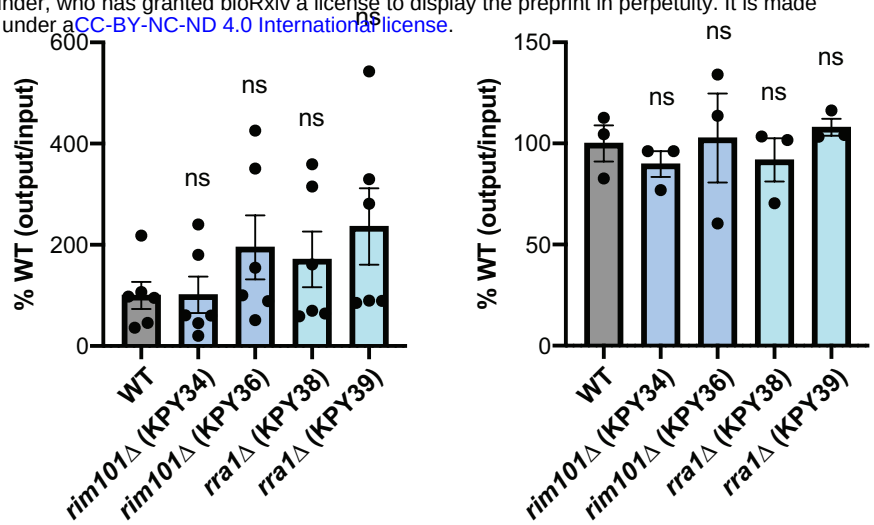

B

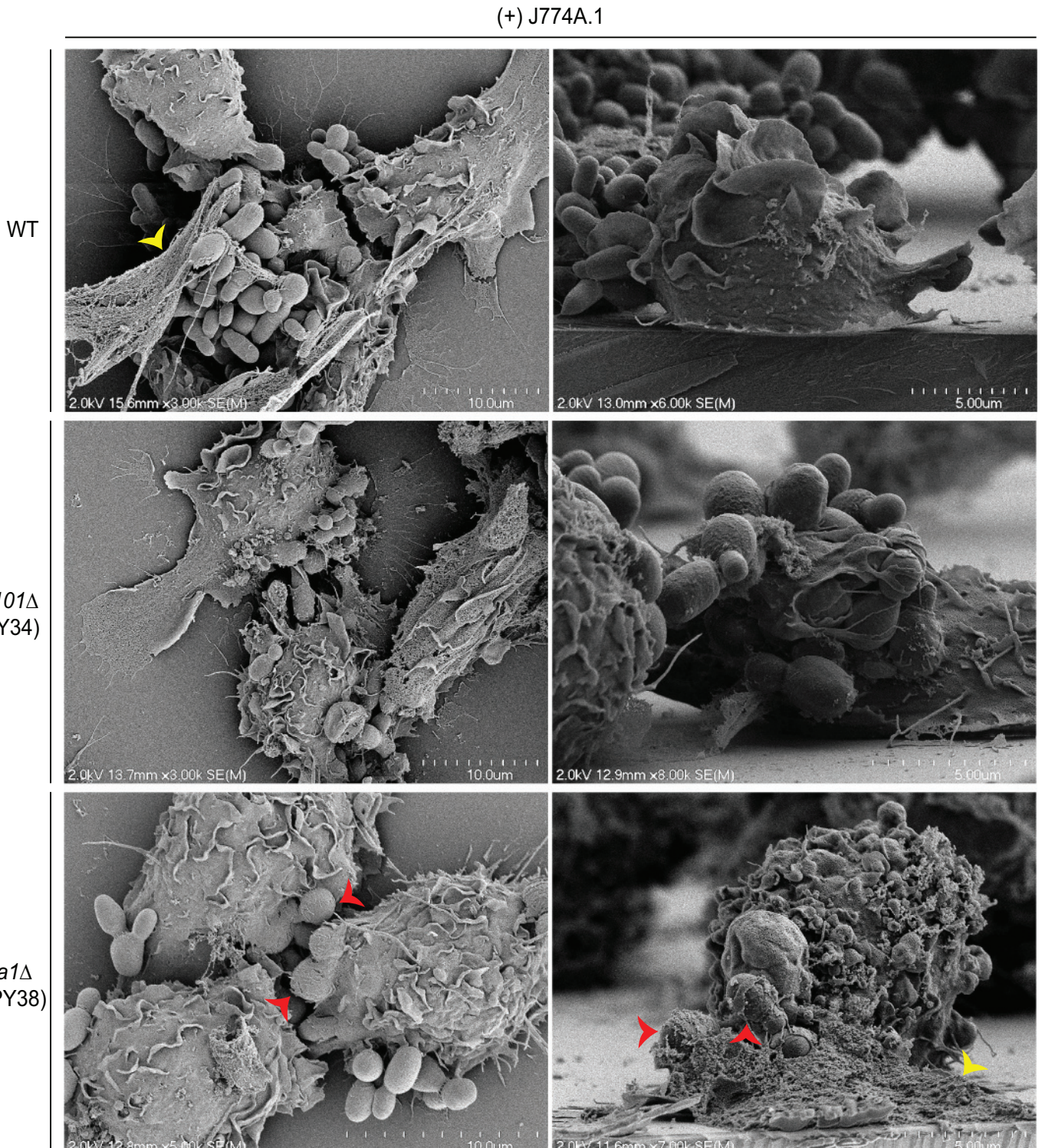

A

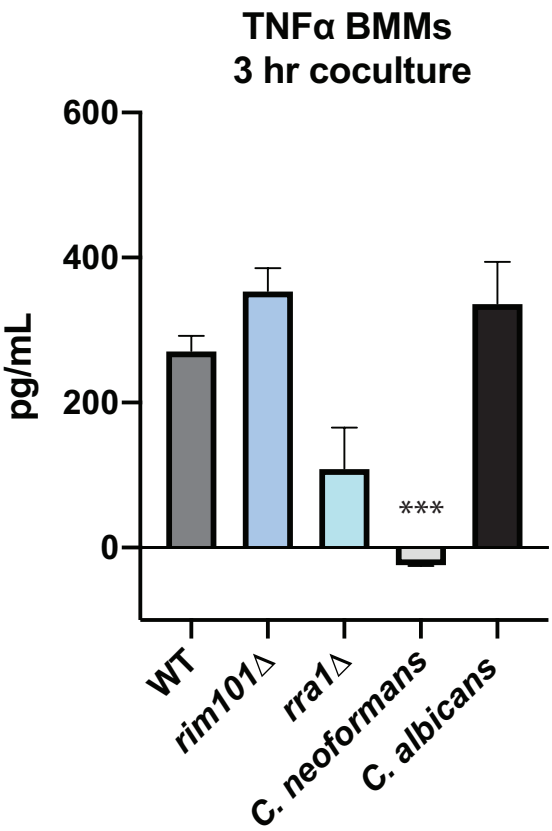
TNFα BMMs
3 hr coculture
600
400
200
0
pg/mL
***
WT
rim101Δ
rra1Δ
C. neoformans
C. albicans

B

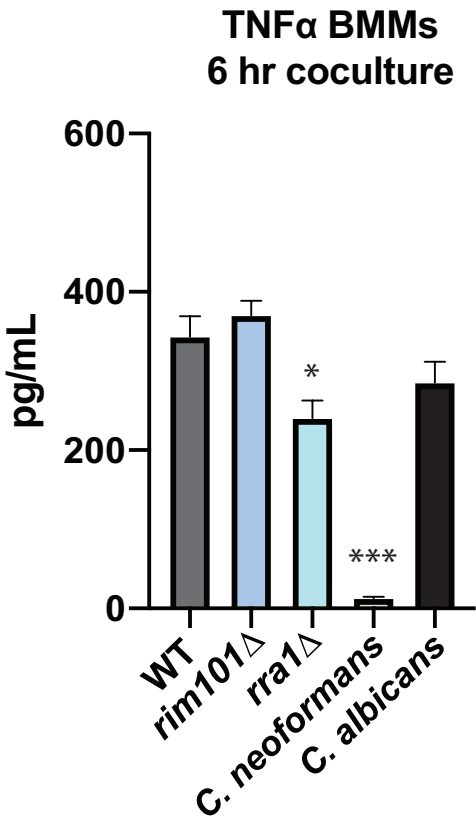
TNFα BMMs
6 hr coculture
600
400
200
0
pg/mL
*
***
WT
rim101Δ
rra1Δ
C. neoformans
C. albicans

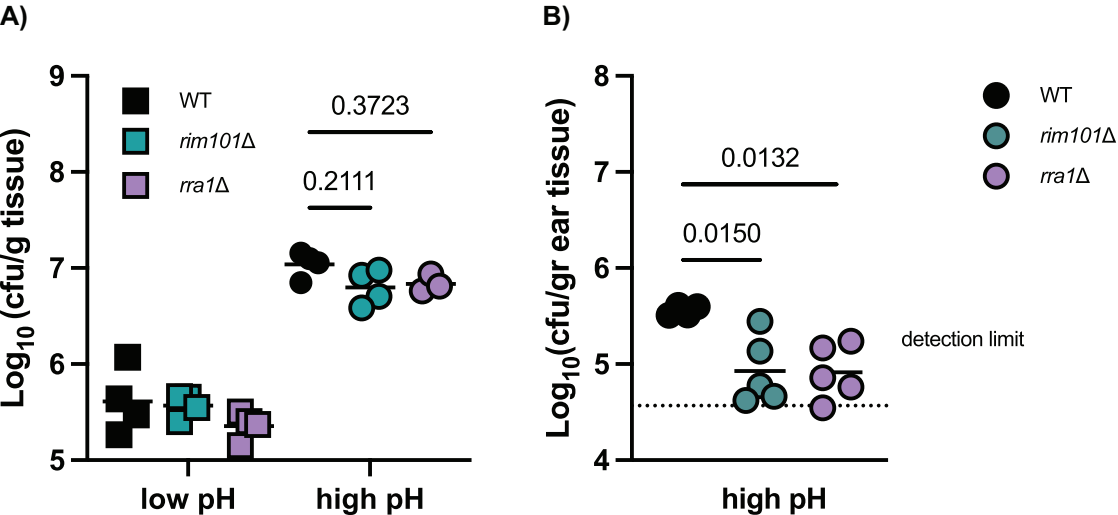
A)
B)
WT
rim101Δ
rra1Δ
0.3723
0.2111
0.0132
0.0150
detection limit
Log10(cfu/g tissue)
Log10(cfu/gr ear tissue)
low pH
high pH
high pH